

# Computational Experiment in the Problem of Supersonic Flow around a Blunt Body with Tail Expansion

I. A. Shirokov<sup>a,\*</sup> and T. G. Elizarova<sup>b</sup>

<sup>a</sup>*Moscow State University, Moscow, 119991 Russia*

<sup>b</sup>*Keldysh Institute of Applied Mathematics, Russian Academy of Sciences, Moscow, 125047 Russia*

\**e-mail: ivanshirokov@inbox.ru*

Received March 4, 2019; revised April 30, 2019; accepted July 1, 2019

**Abstract**—The results of the direct numerical simulation of a supersonic flow around a cylindrical blunt body with tail expansion are presented. The data obtained are compared with the results of laboratory experiments for the Mach numbers 3 and 4 and the angles of attack of 10 and 20 degrees. The results are obtained by using the quasi-gas-dynamic (QGD) equations.

**Keywords:** supersonic flows, quasi-gas-dynamic equations, unstructured spatial grids

**DOI:** 10.1134/S2070048220030163

## 1. INTRODUCTION

The paper presents the results of the 3D direct numerical simulation of four variants of a supersonic flow around an axisymmetric model with the formation of vortex shedding zones near its surface, which can cause the generation of acoustic vibrations. For the selected model, there are laboratory measurements and results of numerical simulations; therefore, this configuration can be considered as a test case for evaluating the accuracy of the numerical approaches. The flow is calculated using quasi-gas-dynamic (QGD) equations without the use of computational procedures with flow limiters traditional for such problems. It was previously shown that a numerical algorithm based on the QGD equations allows us to simulate turbulent flows at low Reynolds and Mach numbers without involving additional turbulence models. In the calculations presented below, turbulence models are also not used.

The aim of the work is to study the possibility of applying the QGD algorithm, implemented on an unstructured tetrahedral computational grid, to model three-dimensional unsteady supersonic viscous gas flows, even using not very good grids.

The model is a cylindrical blunt body with an extension in the tail. The general view and dimensions of the model are shown in Fig. 1 [1].

## 2. STATEMENT OF THE PROBLEM AND GAS-DYNAMIC PARAMETERS

In the bench experiment described in [1], the model is located in the oncoming air flow, while the angle of attack takes values of  $10^\circ$  and  $20^\circ$ . The Mach numbers  $Ma = 3$  and  $Ma = 4$  are considered. The Reynolds number related to the model length 0.127 m equals to  $Re = 6 \times 10^6$  (at  $Ma = 3$ ) and  $Re = 7.6 \times 10^6$  (at  $Ma = 4$ ). Note that the corresponding Reynolds numbers related to 1 m are  $Re_1 = 4.7 \times 10^7$  (at  $Ma = 3$ ) and  $Re_1 = 6 \times 10^7$  (at  $Ma = 4$ ). The free flow parameters have the following values: the gas constant  $R = 287$  J/(kg K), the adiabatic index  $\gamma = 1.4$ , the Prandtl number  $Pr = 14/19$ , and the index of intermolecular interaction  $\omega = 0.74$ .

## 3. MATHEMATICAL MODEL

The system of QGD equations was constructed in [2–4] as a regularized form of the Navier–Stokes (NS) system of equations. The QGD system can be considered as a system of NS equations averaged over

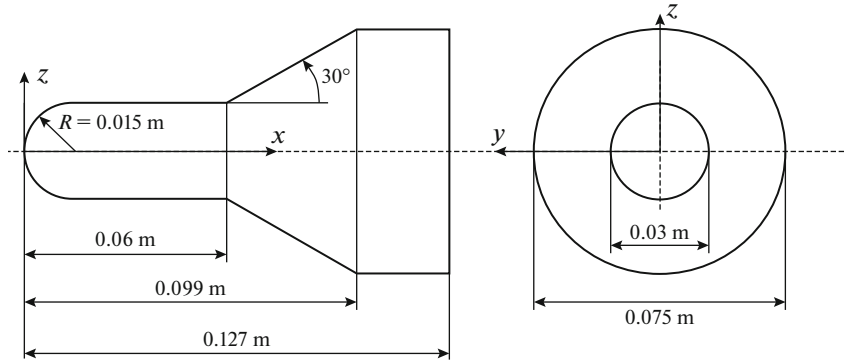


Fig. 1. General view and size of model.

a small space-time interval, which leads to the smoothing (regularization) of the original system of equations.

The QGD system of equations in Cartesian coordinates in the absence of external forces and heat sources can be represented in the form [3]:

$$\frac{\partial}{\partial t} \rho + \nabla_i j_m^i = 0, \quad (1)$$

$$\frac{\partial}{\partial t} \rho u^j + \nabla_i (j_m^i u^j) + \nabla^j p = \nabla_i \Pi^{ij}, \quad (2)$$

$$\frac{\partial}{\partial t} E + \nabla_i (j_m^i H) + \nabla_i q^i = \nabla_i (\Pi^{ij} u_j). \quad (3)$$

Here  $\rho$  is the gas density,  $u^i$  are the components of its macroscopic velocity, and  $p$  is the pressure. The total energy of the unit volume  $E$  and the total specific enthalpy  $H$  of the ideal polytropic gas with the adiabatic exponent  $\gamma$  are calculated by the formulas

$$E = \rho u^2 / 2 + p / (\gamma - 1), \quad H = (E + p) / \rho. \quad (4)$$

The mass flux density vector  $j_m^i$  is defined as

$$j_m^i = \rho (u^i - w^i), \quad w^i = \frac{\tau}{\rho} (\nabla_j \rho u^i u^j + \nabla^i p). \quad (5)$$

The expressions for the viscous stress tensor  $\Pi^{ij}$  and heat flow  $q^i$  are written as

$$\Pi^{ij} = \Pi_{NS}^{ij} + \tau u^i \rho \left( u_k \nabla^k u^j + \frac{1}{\rho} \nabla_j p \right) + \tau \delta^{ij} (u_k \nabla^k p + \gamma p \nabla^k u_k), \quad (6)$$

$$\Pi_{NS}^{ij} = \mu \left( \nabla^i u^j + \nabla^j u^i - \frac{2}{3} \nabla^k u_k \right) + \zeta \delta^{ij} \nabla^k u_k, \quad (7)$$

$$q^i = q_{NS}^i - \tau u^i \rho \left( u_j \nabla^j \varepsilon + p u_j \nabla^j \frac{1}{\rho} \right), \quad q_{NS}^i = -\kappa \nabla^i T. \quad (8)$$

Here  $\varepsilon = p / (\rho(\gamma - 1))$  is the internal energy of a unit mass of gas;  $\Pi_{NS}^{ij}$  and  $q_{NS}^i$  are the viscous stress tensor and heat flux in the NS system;  $\mu$ ,  $\zeta$ , and  $\kappa$  are the coefficients of the shear and bulk viscosity and thermal conductivity, respectively; and  $T$  is the temperature of the gas.

The shear viscosity  $\mu$  is defined via the temperature dependence [3],

$$\mu = \mu_0 (T / T_0)^\omega, \quad (9)$$

where  $\mu_0$  is the gas viscosity coefficient at temperature  $T_0$  and  $0 < \omega < 1$  is the index of intermolecular interaction. The coefficient of bulk viscosity can be calculated using the approximation formula [3]

$$\zeta = \mu((5/3) - \gamma), \quad (10)$$

and the thermal conductivity coefficient is calculated as

$$\kappa = \mu/(\text{Pr}(\gamma - 1)). \quad (11)$$

Coefficient  $\tau$ , which determines additional dissipation in the QGD algorithm, for a viscous polytropic gas has the order of the characteristic time between collisions of the gas particles [2–4]. Its value is associated with the shear viscosity coefficient and can be calculated in the form [3, 4]

$$\tau = \mu/(p \text{Sc}), \quad (12)$$

where  $\text{Sc}$  is the Schmidt number, which for gases is close to unity.

To ensure the stability of the QGD algorithm when modeling supersonic flows of dense gases, it is possible to modify the form of the dissipative coefficient  $\tau$  (12) by including in it a term depending on the spatial grid step and flow parameters in the form

$$\tau = \mu/(p \text{Sc}) + \alpha h/c, \quad (13)$$

where  $h$  is the characteristic size of the spatial cell,  $c$  is the local speed of sound, and  $\alpha$  is a tuning parameter, which in most cases is assumed to be a constant number of the order of 1 [2–5].

However, at high supersonic flow velocities, introduced  $\tau$  viscosity is again insufficient. As the practice of the numerical calculations shows, in these cases, to stabilize the numerical algorithm, it is possible to use the presence of bulk viscosity by introducing an artificial additive in coefficient (10) in the form

$$\zeta = \mu((5/3) - \gamma) + \delta(h/c)p. \quad (14)$$

The value of the regularizing additive here is also determined by the local parameters and depends on the tuning factor  $\delta$ . Such an introduction of artificial dissipation to the QGD equation was first used in [6, 7].

The QGD algorithm is based on system (1)–(8) with dissipative coefficients (9)–(12) and artificial additives (13) and (14).

#### 4. NUMERICAL ALGORITHM

The computational domain is shown in Fig. 2. The incoming air flow is directed towards the positive axis values  $x$  and the free-stream velocity vector lies in the plane  $z = 0$ .

An irregular tetrahedral computational grid is constructed using the freely available TetGen library [8]. Figure 3 shows the general view of the mesh, and Fig. 4 shows a fragment of the mesh in the vicinity of the model at  $z = 0$ . On the surface of the model, the grid elements are rectangular isosceles triangles. The main grid has the following parameters: the total number of nodes is 298 403, there are 1 574 869 tetrahedral elements, and there are 81 312 nodes on the surface of the model. To study the influence of the mesh size on the modeling accuracy, a coarser mesh with the following parameters was used: the total number of nodes was 137 991, there were 732 815 tetrahedral elements, and there were 36 269 nodes on the surface of the model. Thus, the additional mesh is approximately twice as coarse as the main one. As the calculations showed, not only the number of nodes but also the quality of the spatial grid significantly affects the accuracy of the description of the flow fields.

For the numerical modeling, a substantially modified software package was used, created by A.A. Sverdlin and E.M. Kononov [9], which allows the calculation of unsteady viscous gas-dynamic flows for bodies of an arbitrary shape using tetrahedral unstructured spatial grids.

The gas-dynamic parameters (density, viscosity, pressure, temperature, energy) are reduced to dimensionless form. The characteristic length (1 m), density  $\rho_0$ , and speed of sound  $c_0$  in an upstream flow are selected as the dimensional parameters. The values of the gas-dynamic parameters are determined at the grid nodes. The finite-difference approximation of macroscopic QGD equations is constructed using the control volume method. The solution of the initial-boundary-value problem for the grid analogues of QGD equations is found by the explicit in time finite-difference scheme. The spatial derivatives are approximated with a second order of accuracy; and the time derivatives, with the first order accuracy.

The QGD algorithm includes artificial dissipation with tuning factors  $\alpha$  and  $\delta$  (13) and (14). Coefficient  $\alpha = 1$  was considered constant, and the following dependence on the local Mach number was used

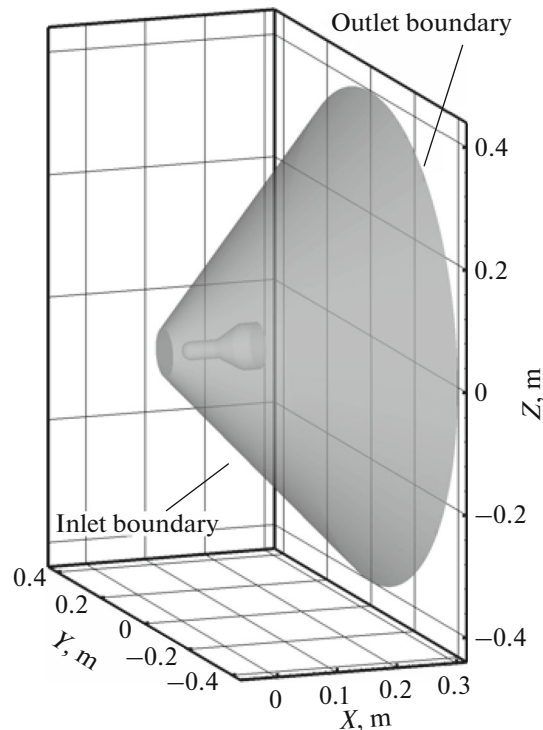


Fig. 2. General view of computational domain.

to calculate coefficient  $\delta$ : for  $Ma \geq 2$ ,  $\delta = 5$ , for  $Ma \leq 1.5$ ,  $\delta = 2$ , in the interval between the values of the Mach numbers 1.5 and 2, coefficient  $\delta$  linearly increases with the Mach number [6].

At the initial moment, the incoming flow parameters are set at the inlet boundary. Inside the computational domain, the same parameters are set except for the velocity: the gas is stationary at the initial moment.

At the inlet boundary, the values of the oncoming flow are kept constant. The soft-boundary conditions are set at the exit boundary; they allow the gas to freely leave the area. The adhesion conditions are set on the solid boundary of the streamlined body (the velocity vector is zero), and the additional boundary condition of the QGD algorithm is used: the normal derivatives of pressure and density are zero [3–5].

As shown by the analytical estimates and the practice of numerical calculations [2–4], the QGD algorithm is stable under the Courant condition. Therefore, the time step is calculated as follows:  $\Delta t = \beta_C h / c$ , where  $\beta_C = 0.1$  is the Courant number,  $h$  is the characteristic local size of the spatial grid, and  $c = \sqrt{T}$  is the local speed of sound.

The calculations were carried out on a multiprocessor K-100 complex [10]. The software complex has good scalability and sufficient parallelization efficiency. In the presented calculations, 128 processor cores were used.

## 5. MODELING RESULTS

Figures 5–8 show in section  $z = 0$  the density profiles for four combinations of the Mach number and the angle of attack ( $AoA$ ) experimentally and numerically investigated in [1]. The streamlines are also shown. Note that the implementation of the QGD algorithm used makes it possible to uniformly conduct modeling in the region entirely surrounding the model, including behind the tail.

Figures 9–11 show the pressure distribution over the surface of the model, referred to the pressure in the unperturbed flow, for the variant  $Ma = 3$ ,  $AoA = 10^\circ$ . Figures 10 and 11 show the projection of the model surface onto the plane  $y = 0$ ; they also show streamlines on the surface. Figure 10 corresponds to the leeward side of the model ( $y > 0$ ); Fig. 11, to the windward side ( $y < 0$ ).

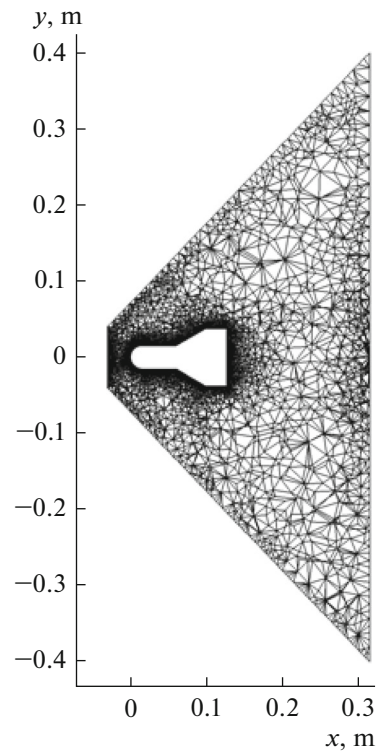


**Fig. 3.** The mesh at  $z = 0$ .

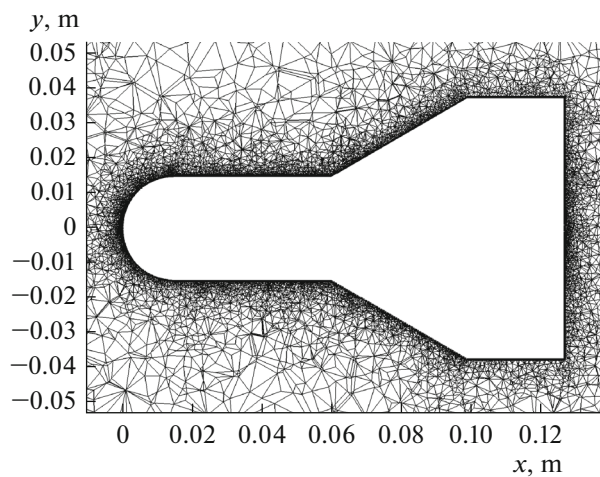


**Fig. 4.** Fragment of the mesh in vicinity of model at  $z = 0$ .

Figure 12 shows one-dimensional pressure profiles on the model surface in the cross section  $z = 0$ , related to the pressure in the undisturbed flow, for the variant  $Ma = 3$  and  $AoA = 10^\circ$ .

The solid line corresponds to the calculation on the main grid with the total number of nodes of 298 403. The dashed line shows the results obtained on an additional, coarser grid with 137 991 nodes. The symbols show the results obtained in an experimental study of the flow around a model in [1]. The experimental data are the pressure values obtained by means of sensors located on the surface of the model.

The triangular symbols correspond to the windward side of the model ( $y < 0$ ); and the square symbols, to the leeward side ( $y > 0$ ). On the whole, we can see a very close agreement between the results obtained

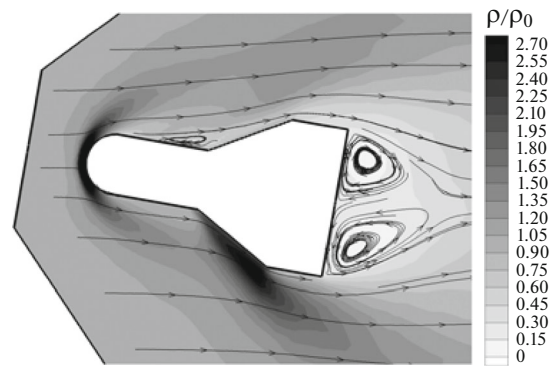


Fig. 5.  $Ma = 3$ ,  $AoA = 10^\circ$ .

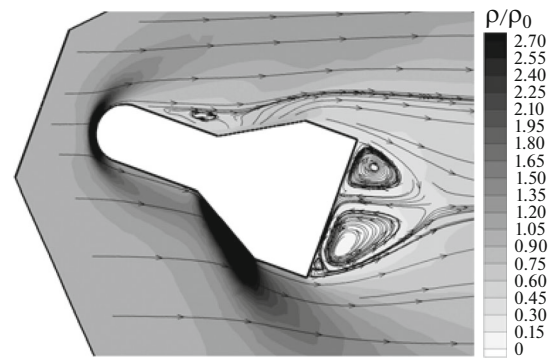


Fig. 6.  $Ma = 3$ ,  $AoA = 20^\circ$ .

in this work and the experimental data. It is also seen that the results obtained on a detailed grid (solid line) are generally closer to the experimental data than those obtained on a coarser grid (dashed line).

The slight overstatement of the maximum pressure in the forward region of the model compared with the experimental one is due to the influence of the grid, since on a more detailed grid the maximum pressure is almost the same as the experimental one. On the windward side of the bow of the model, the simulation results practically coincide with the experimental values. Discrepancies are present in the tail region. Note that in an experimental study of a flow around a model, it is mounted on a bracket, which can affect the flow around the tail region. As for the leeward side of the model, the overestimation of the

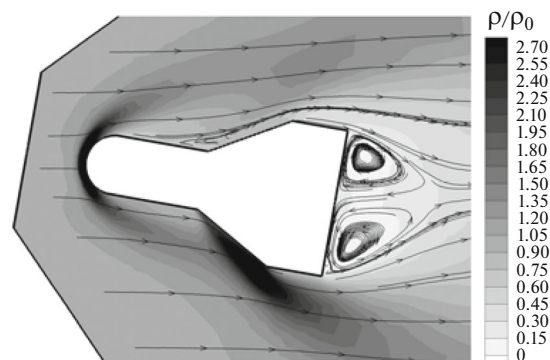


Fig. 7.  $Ma = 4$ ,  $AoA = 10^\circ$ .

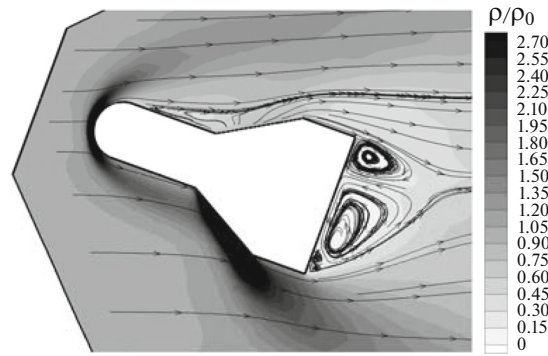


Fig. 8.  $Ma = 4, AoA = 20^\circ$ .

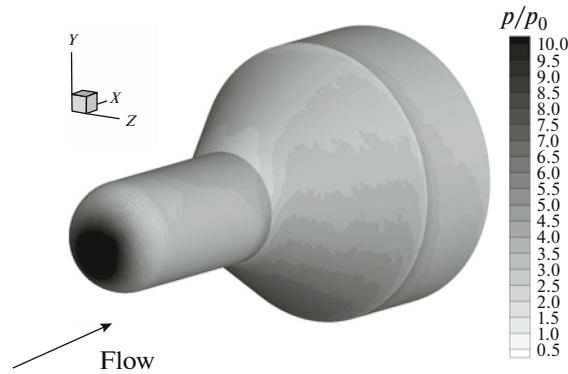


Fig. 9.  $Ma = 3, AoA = 10^\circ$ .

simulation results compared with the experimental data is observed in the area of the bow. In this part there is a swirling motion of the flow.

Note that in the analysis of the simulation results, a non-stationary flow was observed, especially in the vortex region. The capabilities of the QGD algorithm for modeling unsteady flows are also shown in [5].

Figure 13 shows one-dimensional pressure profiles on the model surface in cross section  $z = 0$ , related to the pressure in the undisturbed flow, for the variant  $Ma = 4$  and  $AoA = 20^\circ$ . The results were obtained on the main grid with the 298 403 nodes. The symbols show the results obtained in an experimental study of the flow around a model [1] (the notation is the same as in Fig. 12). Compared to variant  $Ma = 3$ ,

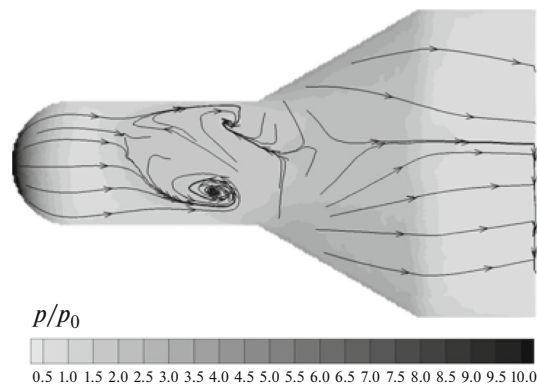


Fig. 10.  $Ma = 3, AoA = 10^\circ$ .

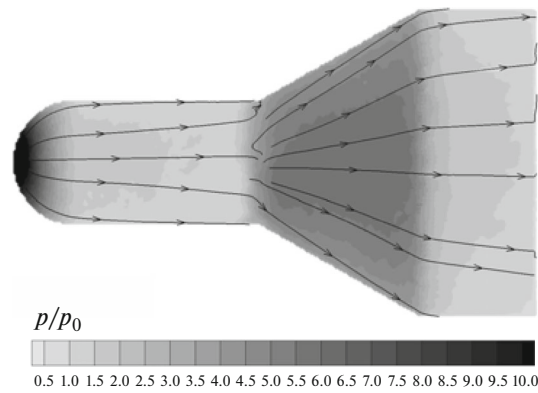


Fig. 11.  $Ma = 3$ ,  $AoA = 10^\circ$ .

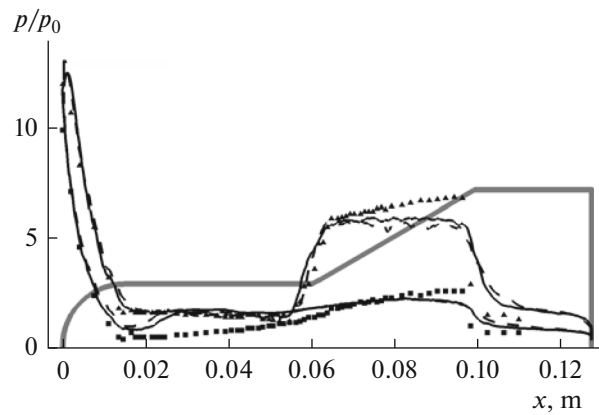


Fig. 12.  $Ma = 3$ ,  $AoA = 10^\circ$ .

$AoA = 10^\circ$  (Fig. 12), the discrepancy between the simulation results and the experiment is greater. This is especially evident in the overestimation of the maximum pressure on the bow, as well as in the absence of a shock wave on the conical part of the model ( $x = 0.08$ ). This is likely to manifest excessive viscosity introduced in the QGD algorithm, as well as a significant irregularity of the relatively coarse mesh used.

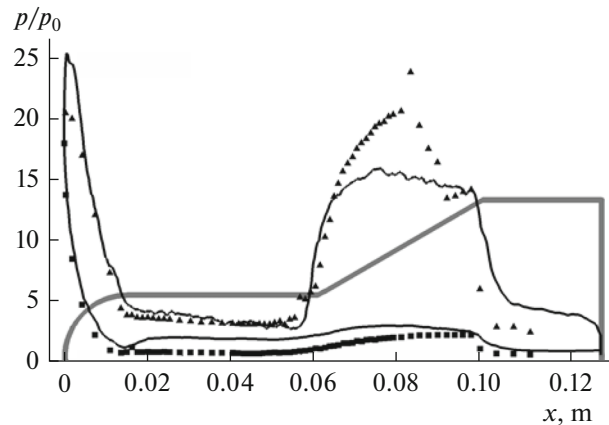


Fig. 13.  $Ma = 4$ ,  $AoA = 20^\circ$ .

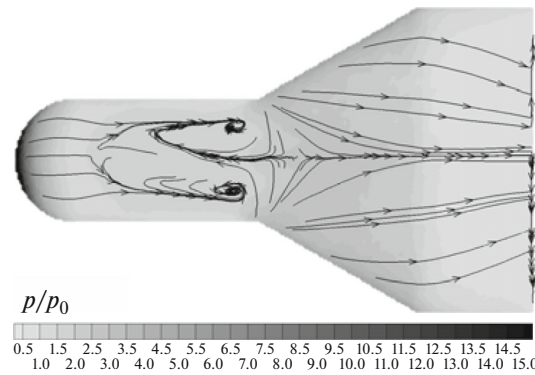


Fig. 14.  $Ma = 4, AoA = 20^\circ$ .

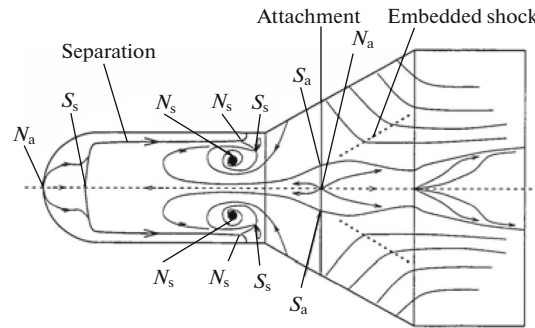


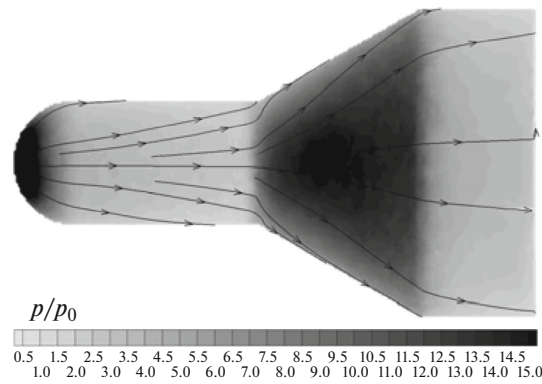
Fig. 15.  $Ma = 4, AoA = 20^\circ$ .

Figure 14, similarly to Fig. 10, depicts the projection of the leeward side ( $y > 0$ ) of the model on the plane  $y = 0$  and the streamlines on the surface, for the variant  $Ma = 4$  and  $AoA = 20^\circ$ . For comparison, Fig. 15 shows a similar projection taken from [1]. It shows the streamlines representing the result of processing the experimental data with the same parameters,  $Ma = 4$  and  $AoA = 20^\circ$ . It can be seen that the experimental picture of the streamlines (Fig. 15) is reproduced in general terms when modeling based on the QGD algorithm (Fig. 14). This is especially noticeable in the arrangement of the paired vortices in front of the conical part of the model.

Figure 16 shows the projection of the leeward side ( $y > 0$ ) of the model on the plane  $y = 0$  and streamlines on the surface for variant  $Ma = 4$  and  $AoA = 20^\circ$ . The vortex motion does not occur in this part of the surface; therefore, the flow pattern is almost symmetrical, as in the analogous Fig. 11. Figure 17 shows an example of the distribution of the computational domain among 128 processors used in one of the calculation variants, in the cross section  $z = 0$ . The total number of steps in the explicit difference scheme for each of the variants is about  $2 \times 10^6$ . The required machine time is about 20 h.

The authors solve the modeling problem in the approximation of the NS equations, taking the viscous terms into account, while the adhesion conditions are on the surface of the body. Thus, the question arises of the resolution of the boundary layer, which is relevant for all numerical algorithms. To clarify this issue in the presented calculations Figs. 18 and 19 show the velocity distribution  $u_x$  near the surface of the model in the cross section of the front cylindrical part  $x = 0.03$  m for variant  $Ma = 4$  and  $AoA = 20^\circ$ . Figure 18 also shows the computational grid. Figure 19 shows a one-dimensional velocity profile  $u_x$  at  $x = 0.03$  m and  $y = 0$ , on which markers are applied corresponding to the boundaries of the mesh cells.

It can be seen that in the boundary layer there are about 7 grid cells. Thus, in modeling, a partial resolution of the boundary layer occurs. Note that the accuracy of the description of the boundary layer is affected not only by the number of points inside it but also by the quality of the grid. The practice of numerical calculations shows that the tetrahedral mesh is not optimal for describing the boundary layer. Nev-



**Fig. 16.**  $Ma = 4$ ,  $AoA = 20^\circ$ .

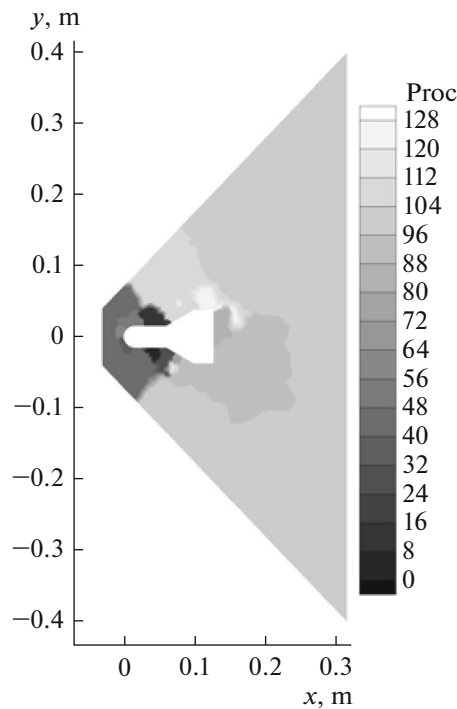


**Fig. 17.** Distribution by processors.

ertheless, even on the low-quality grid used in this work, the QGD algorithm allows one to obtain, on the whole, adequate results of modeling the flow structure and pressure distribution over the model surface.

In [12], a numerical simulation of the supersonic flow around the same model is carried out as in the present work. In this case, the Spalart–Allmaras and SST Menter turbulence models are used and a comparative analysis of the influence of the choice of the model on the flow pattern is carried out. The flow structure obtained in this work (including vortices) and the pressure distribution over the model surface are, on the whole, similar to the results obtained in [12]. However, the structure of the fronts of the shock waves generated in the vicinity of the model in a supersonic flow is better resolved in [12]. Note that in [12], a significantly higher quality and detailed computational grid was used containing 5963967 hexagonal cells (for comparison, in this paper, the grid consists of 1574869 tetrahedra). The practice of numerical calculations shows that the quality of the grid significantly affects the accuracy of the numerical simulation.

One of the versions of the QGD algorithm is included as an additional computing core in the OpenFOAM open source software package [11].

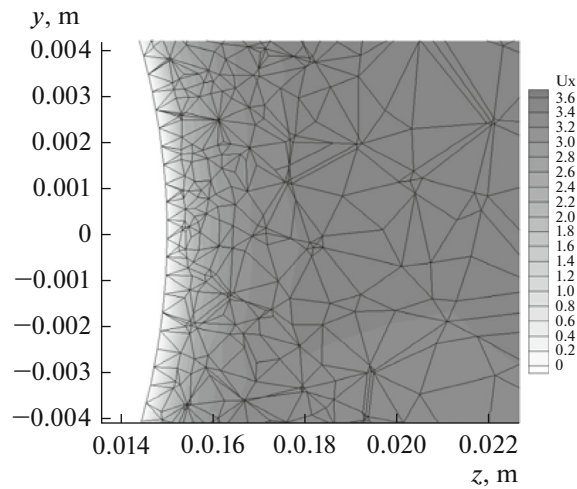


Fig. 18.  $Ma = 4$ ,  $AoA = 20^\circ$ .

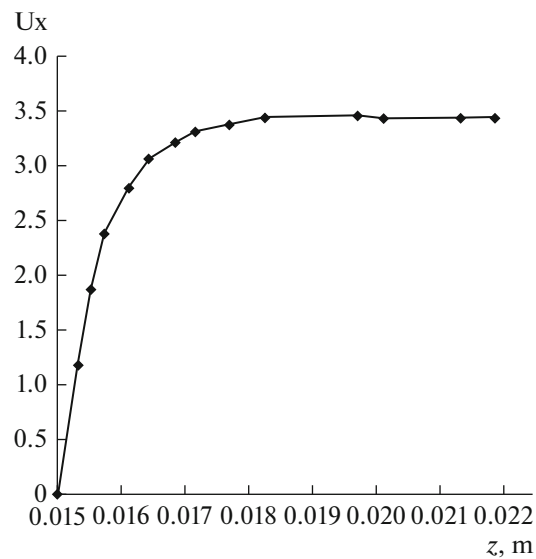


Fig. 19. Velocity profile near surface.

#### ACKNOWLEDGMENTS

The authors thank A.E. Lutsii for his valuable discussion of this topic.

#### FUNDING

This work was supported by the Russian Foundation for Basic Research, project no. 19-01-00262.

#### REFERENCES

1. E. M. Houtman, W. J. Bannink, and B. H. Timmerman, "Experimental and computational study of a blunt cylinder-flare model in high supersonic flow," Report LR-796 (Delft Univ. of Technology, Delft, 1995).
2. B. N. Chetverushkin, *Kinetic Schemes and Quasi-Gas Dynamic System of Equations* (CIMNE, Barcelona, 2008).
3. T. G. Elizarova, *Quasi-Gas Dynamic Equations* (Springer, Dordrecht, 2009),
4. Yu. V. Sheretov, *Regularized Hydrodynamic Equations* (Tver Gos. Univ, Tver', 2016) [in Russian]. <https://elibrary.ru/item.asp?id=30097584>.

5. T. G. Elizarova and I. A. Shirokov, *Regularized Equations and Examples of their Use in the Modeling of Gas-Dynamic Flows* (MAKS-Press, Moscow, 2017) [in Russian]. <https://elibrary.ru/item.asp?id=29352202>
6. I. A. Shirokov and T. G. Elizarova, “Computer simulation of the supersonic flow of a viscous compressible gas around a model body on the basis of the quasi-gas-dynamic algorithm,” *Fiz. Khim. Kinet. Gaz. Dinam.* **18** (2) (2017). <http://chemphys.edu.ru/issues/2017-18-2/articles/721>
7. T. G. Elizarova and I. A. Shirokov, “Artificial dissipation coefficients in regularized equations of supersonic aerodynamics,” *Dokl. Math.* **98**, 648–651 (2018).
8. TetGen: A Quality Tetrahedral Mesh Generator. <http://tetgen.berlios.de/>.
9. T. A. Kudryashova, S. V. Polyakov, and A. A. Sverdlin, “Calculation of gas flow parameters around reentry vehicle,” *Math. Models Comput. Simul.* **1**, 445–452 (2009).
10. K-100 System, Keldysh Inst. Appl. Math. RAS, Moscow. <http://www.kiam.ru/MVS/resourses/k100.htm>.
11. M. V. Kraposhin, E. V. Smirnova, T. G. Elizarova, and M. A. Istomina, “Development of a new OpenFOAM solver using regularized gas-dynamic equations,” *Comput. Fluids* **166**, 163–175 (2018).
12. V. E. Borisov, A. A. Davydov, A. E. Lutskii, and Ya. V. Khankhasaeva, “Numerical study of the flow around spacecraft model,” KIAM Preprint No. 130 (Keldysh Inst. Appl. Math., Moscow, 2017). <http://library.keldysh.ru/preprint.asp?id=2017-130>. <https://doi.org/10.20948/prepr-2017-130>